GDCh

Research Articles

Angewandte
Chemie
International Edition
www.angewandte.org

Ammonia Synthesis

Approach to Chemically Durable Nickel and Cobalt Lanthanum-Nitride-Based Catalysts for Ammonia Synthesis

Yangfan Lu[+],* Tian-Nan Ye[+], Jiang Li[+], Zichuang Li, Haotian Guan, Masato Sasase, Yasuhiro Niwa, Hitoshi Abe, Qian Li, Fushen Pan, Masaaki Kitano,* and Hideo Hosono*

Abstract: Metal nitride complexes have recently been proposed as an efficient noble-metal-free catalyst for ammonia synthesis utilizing a dual active site concept. However, their high sensitivity to air and moisture has restricted potential applications. We report that their chemical sensitivity can be improved by introducing Al into the LaN lattice, thereby forming La–Al metallic bonds (La–Al–N). The catalytic activity and mechanism of the resulting *TM*/La–Al–N (*TM* = Ni, Co) are comparable to the previously reported *TM*/LaN catalyst. Notably, the catalytic activity did not degrade after exposure to air and moisture. Kinetic analysis and isotopic experiment showed that La–Al–N is responsible for N₂ absorption and activation despite substantial Al being introduced into its lattice because the local coordination of the lattice N remained largely unchanged. These findings show the effectiveness of metallic bond formation, which can support the chemical stability of rare-earth nitrides with retention of catalytic functionality.

Introduction

While ammonia is an important intermediate to produce chemicals and fertilizers worldwide, the ammonia synthesis reaction has long-suffered from dissociation of nitrogen molecules (N₂) because of its large N≡N bond energy (945 kJ mol⁻¹).[1–3] After the milestone development of the Haber-Bosch process, numerous studies have been conducted to realize ammonia synthesis under milder reaction conditions. One of the recent successful examples includes electride-based catalysts, such as Ru-loaded $[Ca_{24}Al_{28}O_{64}]^{4+}$ (e⁻)₄ (Ru/C12A7:e⁻).[4–7] Electride-based catalysts are characterized by strong electron donation ability and interactions between supports and active metals.[5,8] Low work function electrons inherent to C12A7:e⁻ can be efficiently transferred to the anti-bonding LUMO state of N₂ molecules, realizing lower activation energy (E_a) of ammonia synthesis.[5,9,10] The low E_a nature can be universally observed in electride-based catalysts, including Ru/Y₅Si₃ and Ru/LaScSi, and their TOFs become one or two orders of magnitude greater than that of traditional ones.[11,12] It is another advantage of using electrides as supports that hydrogen poisoning common to Ru-catalyst is suppressed based on the smooth exchange between the anionic electron and adatom hydrogen formed on Ru.[13] The success of electride-based catalysts demonstrates the importance of allowing supports to participate in the catalytic mechanism.

In ammonia synthesis catalysts, Ru catalysts have drawn considerable attention because they support an optimal *TM*-N (*TM*: transition metals) interaction, while the other more affordable transition metals, such as Ni, are less effective because its *TM*-N interactions are either too strong to promote N–H formation or too weak to serve as an active center.[14–17] This limitation is widely known as a scaling

---

[*] Prof. Y. Lu,[+] H. Guan, Prof. Q. Li, Prof. F. Pan
College of Materials Science and Engineering, National Engineering Research Center for Magnesium Alloys, Chongqing University
Chongqing 400044 (China)
E-mail: yangfanlu@cqu.edu.cn

Prof. T.-N. Ye,[+] Z. Li
Frontiers Science Center for Transformative Molecules, School of Chemistry and Chemical Engineering, Shanghai Jiao Tong University
Shanghai 200240 (China)

Dr. J. Li,[+] Dr. M. Sasase, Prof. M. Kitano, Prof. H. Hosono
Materials Research Center for Element Strategy, Tokyo Institute of Technology
4259 Nagatsuta, Midori-ku, Yokohama 226-8503 (Japan)
E-mail: kitano.m.aa@m.titech.ac.jp
      hosono@mces.titech.ac.jp

Dr. Y. Niwa, Prof. H. Abe
Institute of Materials Structure Science, High Energy Accelerator Research Organization
Tsukuba, Ibaraki 305-0801 (Japan)

Dr. Y. Niwa, Prof. H. Abe
Department of Materials Structure Science, School of High Energy Accelerator Science, SOKENDAI, The Graduate University for Advanced Studies
Tsukuba, Ibaraki 305-0801 (Japan)

Prof. H. Abe
Graduate School of Science and Engineering, Ibaraki University
Mito, Ibaraki 310-8512 (Japan)

Prof. Q. Li
State Key Laboratory of Advanced Special Steel, Shanghai Key Laboratory of Advanced Ferro-metallurgy, School of Materials Science and Engineering, Shanghai University
Shanghai 200444 (China)

[+] These authors contributed equally to this work.

---

relation.[18–21] In order to overcome this difficulty, the catalytic functionalities arising from the combination between transition metals and supports has drawn attention. For example, Chen et al. reported that LiH combined with transition metals work as efficient catalysts for ammonia synthesis.[22,23] In it, ubiquitous elements, such as Mn and Fe, are applicable for low-temperature ammonia synthesis because the dissociated nitrogen can react with the lattice hydrogen of LiH to produce ammonia. The importance of the supports' contributions to ammonia synthesis has been further explored in nitride-based catalysts, including (Co,Ni)–Mo–N, Ru/TiCN/ZrH$_2$, Ru/LaN/ZrH$_2$ and Co–N–C.[24–28] These catalysts show high catalytic activities for ammonia production because of the contribution of lattice nitrogen in the catalytic cycles, which can significantly enhance N$_2$ absorption and activation processes.

These studies revealed the advantages of combining active metals and supports, either electronically or structurally, to extend the degree of freedom of material design and achieve desired functionalities, which can be applied to ammonia synthesis and other chemical reactions.[29–31] In this context, we have recently reported the Ni-based ammonia synthesis catalyst, Ni/ReN (Re = La, Ce).[32,33] While Ni has long been believed to be a poor catalyst for ammonia synthesis due to its weak Ni–N interaction,[19–21] it became possible to overcome the scaling relations with the dual active sites mechanism. In Ni/ReN, nitrogen in NRe$_6$ octahedra efficiently react with hydrogen atoms dissociated by Ni catalysts, forming NH$_3$ and nitrogen vacancies. The vacancies can absorb and activate N$_2$ molecules instead of loaded metal catalysts, realizing efficient and low-cost catalysts. However, the high sensitivity of ReN towards air and moisture poses major challenges for further practical applications.[32,33]

How can we address the chemical instability of rare-earth nitrides without affecting their catalytic functionalities? We are aware that some of the rare-earth materials include intermetallics, which exhibit excellent chemical stability. For example, a rare-earth-rich intermetallic compound, Re$_{16}$(Au$_x$Al$_{13-x}$), was reported to be air and moisture stable for months.[34] LaRuSi and LaPtSi$_2$ are even stable in acid aqueous solution.[35–37] Thus, we considered that chemical stability would be improved through chemical bond formation between rare-earth and counter elements. We believed that it would be possible to create a new noble metal-free catalyst for ammonia synthesis that is stable in air and moisture for materials co-hosting nitrogen local coordination identical to that of ReN (NRe$_6$ octahedra) and Re-M metallic bonds.

Herein, we report that La$_3$AlN is one of the materials which can achieve the research objectives described above. By loading Ni and Co, the composite decomposed to Al-doped LaN (La–Al–N) and continuously produced NH$_3$ for at least 80 h, with reaction rates of 2410 μmol g^{-1}h^{-1} for Ni/La–Al–N under 0.1 MPa and 400°C. Isotope experiments demonstrated that the dual active site mechanism (associative route) is also available in this system; i.e., the La–N–Al support keeps contributing to activate N$_2$ molecule to realize a stable catalytic cycle. The catalytic activity can be further enhanced by changing Ni to Co (2735 μmol g^{-1}h^{-1}) because Co offers extra active sites for nitrogen activation. Notably,

the Ni- and Co-loaded La–Al–N catalysts show no distinct degradation after air and moisture exposure. These discoveries show the importance of metallic bond formation, allowing the rare-earth nitride composite to simultaneously support chemical stability and efficient catalytic activity.

Results and Discussion

Figure 1a shows the crystal structure of LaN and La$_3$AlN. LaN crystallizes in the rock-salt-type structure and its nitrogen is octahedrally coordinated by six La atoms, forming NLa$_6$ octahedral coordination. Meanwhile, La$_3$AlN is one of the anti-perovskite compounds; in contrast to the standard perovskite like SrTiO$_3$ in which Ti is octahedrally coordinated by O (TiO$_6$ octahedra), the coordination is reversed in La$_3$AlN.[38] In the "inversed" structure, Al occupies the position of Sr, N occupies the Ti site, and La the O site. The local coordination of nitrogen thus remains identical to that of LaN. In addition, the La forms a metallic bond with Al with a bond length of ≈3.6 Å, which is comparable to that of La–Al binary intermetallics.[34,39,40] As shown in Figure 1b, despite the fact that La$_3$AlN is a rare-earth-rich material, its powder X-ray diffraction (XRD) pattern and intensity remained largely unchanged after exposure to air for 1 hour. This observation is in stark contrast to the case of LaN, which transforms to La(OH)$_3$ in air within a few minutes (Figure 1b), demonstrating the effectiveness of La–Al bonding to protect the material against hydration.
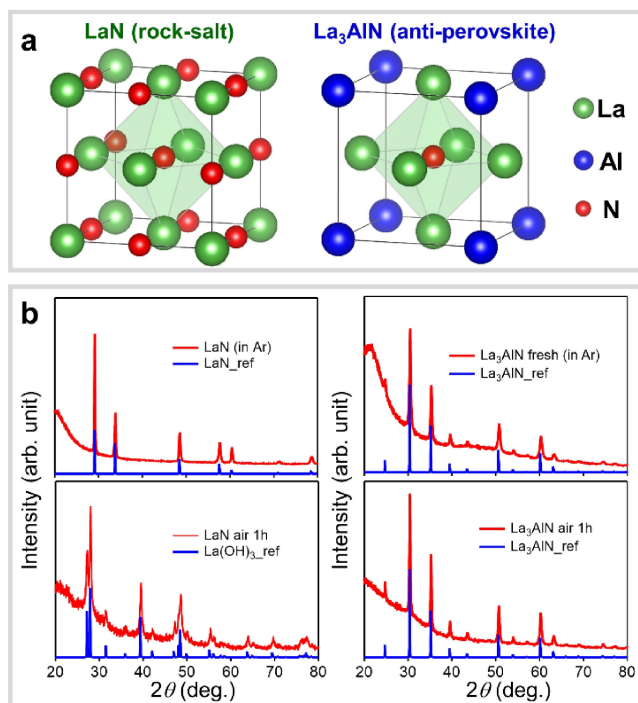
Figure 1. a) The crystal structure for LaN and La$_3$AlN. b) The powder XRD pattern for LaN and La$_3$AlN before and after exposure to air for 1 hour.

Angew. Chem. Int. Ed. **2022**, 61, e202211759 (2 of 7)

© 2022 Wiley-VCH GmbH

Motivated by the presence of NLa$_6$ octahedral coordination and improved air durability, we subsequently applied La$_3$AlN to the catalyst for ammonia synthesis by loading Ni on its surface. In this paper, we represent these catalysts as *TM*/La–Al–N because La$_3$AlN changes its nitrogen content and structure after the ammonia synthesis, which will be discussed later. The metal loading amount of Ni and Co was set to 5 wt% for *TM*/La–Al–N. A 5 wt% metal loading was employed because the metal:support ratio was reported as the optimized point for the *Re*N bulk catalyst, which has a similar particle size to the presented La–Al–N, allowing us to compare the properties of each system.[32,33] The particle sizes of Ni and Co were respectively estimated to be 39.2 nm and 18.4 nm, giving dispersion of 0.6% and 1.4%, respectively (Figure S1). As shown in Figure 2a and 2b, the catalytic activity and activation energy for the Ni/La–Al–N catalyst was measured to be 2410 µmol g^{-1} h^{-1} (400°C) and 58 kJ mol^{-1} under 0.1 MPa, and 5131 µmol g^{-1} h^{-1} (400°C) and 67 kJ mol^{-1} under 0.9 MPa, which is comparable to that of the bulk Ni/LaN catalyst with a similar surface area, S_{BET} (S_{BET} = 1.9 m^2 g^{-1} for Ni/LaN; S_{BET} = 3.8 m^2 g^{-1} for Ni/La–Al–N). The catalytic activity can be enhanced by changing Ni to Co. In the case of Co/La–Al–N, the catalytic activities were 2735 µmol g^{-1} h^{-1} for 0.1 MPa and 8456 µmol g^{-1} h^{-1} for 0.9 MPa under 400°C, and its activation energy was estimated to be 44 kJ mol^{-1} (0.1 MPa) and 49 kJ mol^{-1} (0.9 MPa) (Figure 2c and 2d). The catalytic activities and high-pressure effects were well reproduced over the different batches of samples (Figure S2), and both Ni- and Co-loaded catalysts continuously produced ammonia for at least 80 hours without obvious degradation. The estimated activation energies are smaller than traditional catalysts (e.g., Cs–Ru/MgO, ≈86 kJ mol^{-1}),[4] demonstrating that the N$_2$ activation process was significantly enhanced. The reaction orders were estimated to be α (N$_2$) = 1.0, β (H$_2$) = 1.2, and γ (NH$_3$) = −1.2 for Ni/La–Al–N and α (N$_2$) = 1.1, β (H$_2$) = 1.6, and γ (NH$_3$) = −1.3 for Co/La–Al–N, respectively (Figure S3). The higher reaction order of H$_2$ (β) for Co/La–Al–N resulted in a better high-pressure effect for Co/La–Al–N. These data are comparable to those of previously reported Ni- and Co-loaded *Re*N,[32,33,41] suggesting that a dual active site mechanism is available for Ni/La–Al–N and Co/La–Al–N.
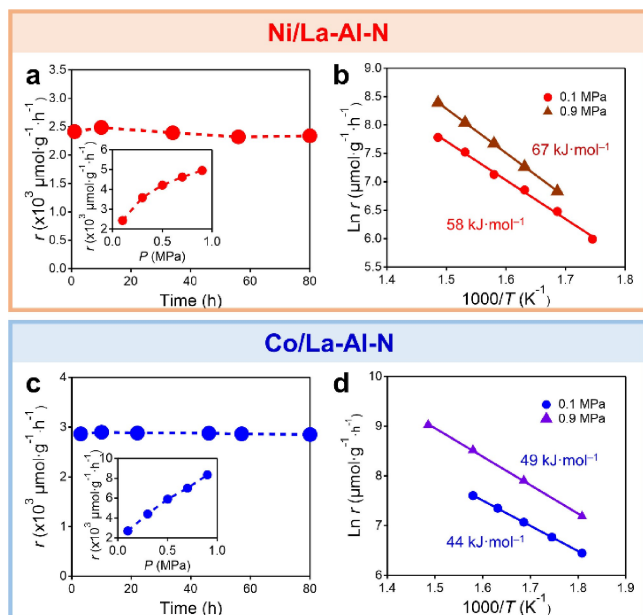
To unveil their reaction mechanisms, we subsequently conducted isotope experiments by using ^{15}N$_2$ (Figure 3). We note that the Ni- and Co-loaded La–Al–N initially contains ^{14}N in its lattice. When the reaction proceeds in a ^{15}N$_2$ and H$_2$ atmosphere, the m/z = 30 (^{15}N$_2$) signal decreases, while m/z = 18 (^{15}NH$_3$) and 17 (^{15}NH$_2$, ^{14}NH$_3$) increase. The intensity rates, (m/z = 17)/(m/z = 18) and (m/z = 16)/(m/z = 18), were as high as 1.0 and 0.2 initially, and finally decreased to 0.8 and 0.075, which were consistent with the theoretical values.[42] The deviation of the fragment ratio demonstrated that the generation of NH$_3$ was derived from both ^{15}NH$_3$ and ^{14}NH$_3$,[42] indicating that ^{14}N in the La–Al–N lattice was involved in the catalytic cycle. The slightly lower ^{15}N$_2$ conversion rate of Co/La–Al–N compared to that of Ni/La–Al–N is attributed to the pressure effect of these two catalysts. As shown in the inset of Figure 2a and 2c, the high-pressure effect of the Co/La–Al–N catalyst is more significant than that for the Ni/La–Al–N catalyst. In other words, the ammonia production rate of Co/La–Al–N can be suppressed to a greater extent under lower pressure conditions. Since the isotope experiments were conducted under 0.06 MPa, the ^{15}N$_2$ consumption in the Co/La–Al–N catalyst became lower than that of Ni/La–Al–N.

Figure 2. a) Catalytic activity and b) Arrhenius plot for Ni/La–N–Al. Identical data for Co/La–N–Al are shown in c) and d). The insets of (a) and (c) represent the high-pressure effects of each catalyst.
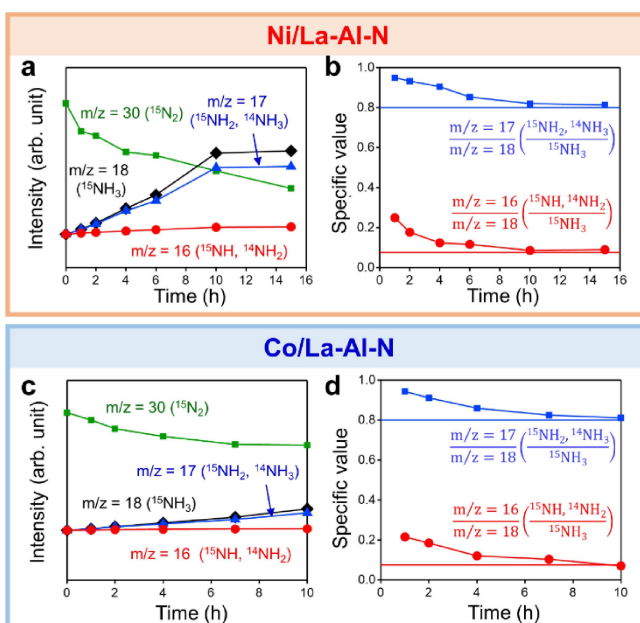
Figure 3. Ammonia synthesis from ^{15}N$_2$ and H$_2$ over a) Ni/La–Al–N and c) Co/La–Al–N. Reaction time profiles for the ratio changes of 17/18 and 16/18 of each catalyst are shown in (c) and (d). For the pure ^{15}NH$_3$ gas, the ration values of ^{15}NH$_2$/^{15}NH$_3$ (17/18) and ^{15}NH/^{15}NH$_3$ (16/18) are 0.8 and 0.075, respectively.

We also tested the catalytic activity over the nitrogen isotope exchange reaction, $^{14}N_2 + {}^{15}N_2 \rightarrow 2{}^{14}N^{15}N$ (Figure S4). For Ni/La–Al–N, the $^{14}N^{15}N$ production rate was as high as $\approx 100\ \mu mol\,g^{-1}\,h^{-1}$ with an activation energy of $125\ kJ\,mol^{-1}$, which is comparable to that of Ni/LaN. Given the fact that the other Ni-loaded catalysts, such as Ni/C12A7:e$^-$, do not show activity for the nitrogen exchange reaction, these results suggest that lattice nitrogen and its La–Al–N defect plays a key role in N_2 adsorption, in which the La–Al–N support and Ni are respectively responsible for N_2 and H_2 absorption and activation. When the active metal is changed from Ni to Co, the $^{14}N^{15}N$ production rate reaches $\approx 420\ \mu mol\,g^{-1}\,h^{-1}$ with an activation energy of $122\ kJ\,mol^{-1}$. The rate value is four times greater than that for Ni-loaded La–Al–N, and even higher than that for Co/C12A7:e$^-$, indicating that loaded Co metal can also activate N_2 molecules. This fact suggests that the conventional dissociative route can be available for Co/La–Al–N.

To confirm the catalytic mechanism, temperature-programmed surface reaction (TPSR) measurements were conducted under N_2-D_2 and Ar-D_2 atmospheres. Both catalysts were treated under ammonia synthesis conditions before the measurements. Therefore, the catalyst surface contained ^{14}N and ^1H species. Figure S5 shows the TPSR results of Ni/La–Al–N and Co/La–Al–N under an N_2/D_2 atmosphere. Ammonia-isotope-related species for $m/z = 20$ (ND_3), 19 (ND_2H), 18 (NDH_2, ND_2), 17 (NDH, NH_3), and 16 (NH_2) were identified in these measurements respectively. For the case of Ni/La–Al–N (black line), a drastic increase of ammonia-related isotope effects can be observed at around 350–400 °C. Given the fact that Ni is unlikely to absorb and activate N_2 molecules, the peak is attributed to the ammonia production under the associative route. Notably, two peaks can be observed for the TPSR spectrum of Co/La–Al–N, as emphasized by the blue solid arrows in Figure S5 (red line). In addition to the peak located at round 350–400 °C, smaller but clear signals can be found in the lower temperature (≈ 150 °C) region. A similar tendency was also found for the Ar/D_2 TPSR spectra. Figure 4 presents Ar/D_2 TPSR spectra for Ni/La–Al–N and Co/La–Al–N. In the case of Ni/La–Al–N, a major peak emerges at ≈ 400 °C, which is associated with $m/z = 17$ ($^{14}NH_3$, ^{14}NDH) and $m/z = 18$ ($^{14}NDH_2$, $^{14}ND_2$) (Figure 4a). These peak positions are consistent with previously reported H_2-TPR measurements for Ni/ReN, in which major peaks at $m/z = 17$ (NH_3) appeared in the range of 350–400 °C.[33] The peak is attributed to the process in which the dissociated D reacts with the lattice nitrogen of La–Al–N to form N–D_x species and a nitrogen-vacancy. In combination with the $^{14}N_2/{}^{15}N_2$ exchange reaction experiments, it is concluded that lattice N and N vacancies contribute to the ammonia synthesis reaction in the catalytic cycle of Ni/La–Al–N (associative route) (Figure 4b). In contrast, two peaks were identified for Co/La–Al–N (Figure 4c). The peak at higher temperature is consistent with the peak observed for Ni/La–Al–N, suggesting that dissociated D species can also react with lattice nitrogen in Co/La–Al–N through the associative mechanism. Meanwhile, the TPSR spectrum of Co/La–Al–N presents a clearer peak at a lower temperature (≈ 150 °C). This spectral structure is consistent with the case of
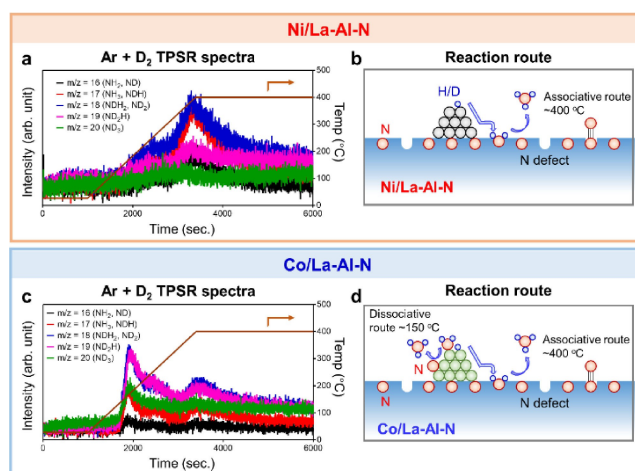
Figure 4. Ar/D_2 TPSR spectra of a) Ni/La–Al–N and c) Co/La–Al–N. The mass of different species are shown by black ($m/z = 16$), red ($m/z = 17$), blue ($m/z = 18$), pink ($m/z = 19$), and green ($m/z = 20$) solid lines, respectively. Panels b) and d) illustrate the catalytic mechanisms in Ni- and Co-loaded La–Al–N.

Co/CeN,[41] in which ammonia can be produced under both associative and conventional dissociative mechanisms. The lower temperature peak is associated with the reaction between dissociated D and N on the Co surface, indicating that both dissociative and associative routes are available for Co/La–Al–N (Figure 4d). Therefore, Co/La–Al–N offers more catalytically active sites, realizing a higher ammonia production rate. The associative and dissociative concerted mechanism is also supported by $^{14}N_2/{}^{15}N_2$ exchange reaction experiments over Co/La–Al–N, showing a much higher $^{14}N^{15}N$ production rate than that of Ni/La–Al–N.

Notably, a similar reaction mechanism, in which lattice nitrogen participates in the catalytic cycle, was reported for various nitride-based catalysts. Well-known examples include the Co–Mo–N[27] and Ni–Mo–N[28] ternary systems. The literature suggests that the nitrogen of their lattice is involved in ammonia production. The discoveries of Co–N–C,[24] Ru/LaN/ZrH$_2$,[26] and TM/ReN systems[32,33] further demonstrate the contribution of lattice nitrogen, as well as its vacancies, to N_2 activation, with much improved catalytic activities in ammonia synthesis. In this work, the activation energies of TM/La–Al–N were comparable to previously reported Co/CeN[41] ($45\ kJ\,mol^{-1}$ at 0.9 MPa), Co–N–C,[24] ($50\ kJ\,mol^{-1}$ at 1.0 MPa), and Ru/3LaN/ZrH$_2$[26] ($64\ kJ\,mol^{-1}$ at 1.0 MPa), showing that the activation barrier of the rate-determining step was significantly suppressed by utilizing a nitride support.

While the presented catalysts exhibit comparable activity and a similar mechanism to TM/ReN catalysts, the improved chemical durability should be highlighted. Figure 5 presents the moisture exposure tests of TM/La–Al–N. We first conducted conventional ammonia synthesis and introduced moist N_2 into the reactor at room temperature for 1 hour. The moisture was introduced by bubbling N_2 gas in a water bath, and thus, the feed gas contains ≈ 34000 ppm of H_2O (Figure 5a). Similar moisture–exposure experiments were also
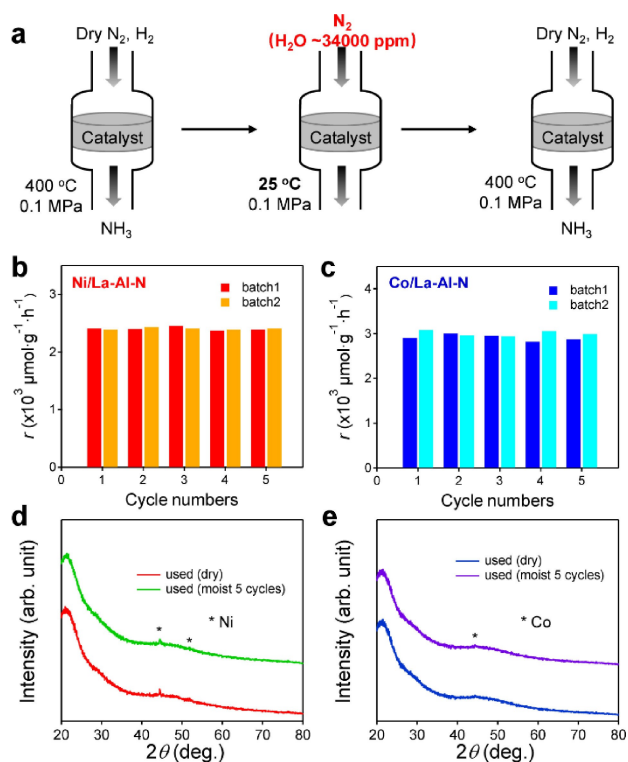
Figure 5. a) Illustration of the moisture exposure process. The cycle properties of moisture exposure are shown in b) for Ni/La–Al–N and c) for Co/La–Al–N. Two batches of samples were tested for the moisture exposure experiments. The powder XRD patterns for d) used Ni/La–Al–N and e) used Co/La–Al–N. Both powder XRD patterns for moisture-exposed and non-exposed samples are shown.

employed for previous studies of Ru/Y_5Si_3 and Ru/LaScSi.[11,12] For the case of Ni/LaN, it lost catalytic activity and transformed to Ni/La_2O_3 after a single moisture exposure process (Figure S6). LaN transforms to La(OH)$_3$ by reacting with introduced H_2O and then becomes La_2O_3 after ammonia synthesis under N_2/H_2 at 400 °C. We are also aware that Chen et al. conducted a similar stability test in which Li_4RuH_6/MgO and Ba_2RuH_6/MgO were exposed to air, resulting in a substantial degradation of catalytic activities.[43] Meanwhile, neither Ni- nor Co-loaded La–Al–N experienced a degradation in catalytic activity, even after five cycles of moisture exposure. The moisture durability could be reproduced over the different batches of samples (Figure 5b and 5c). In addition, we conducted a catalytic durability test for *TM*/La–Al–N by changing the H_2O content during the ammonia synthesis reaction. Notably, we used a high-purity feed gas in which H_2O content is lower than 0.01 ppm in the previous measurements. We subsequently introduced 3–5 ppm of H_2O to the feed gas and compared the catalytic activity and durability. A 3–5 ppm dose of H_2O was introduced into the feed gas because it satisfies the standards of industrial nitrogen gas (JIS K1107), in which the H_2O content is set to be lower than 5.3 ppm. As shown in Figure S7, the catalytic activities of *TM*/La–Al–N were 2–3 % (Ni) and 6–7 % (Co), which was suppressed by introducing 3–5 ppm of H_2O to the feed gas but retained stable ammonia production. Importantly, the catalytic

activity recovered by switching the feed gas to a high-purity grade, which demonstrates the high chemical stability of *TM*/La–Al–N well.

Interestingly, the crystal structure and chemical composition of the catalysts drastically changed after ammonia production. It is shown that both Ni- and Co-loaded La–Al–N turn into an amorphous-like structure and only the peaks originating from Ni and Co metals could be observed (Figure 5d and 5e). Electron probe micro analyzer (EPMA) measurements revealed that the chemical compositions changed from $La_3Al_{0.78}N_{1.02}$ to $La_3Al_{0.80}N_{3.54}$ for Ni-loaded system and $La_3Al_{0.77}N_{4.41}$ for Co-loaded systems, drastically increasing the nitrogen content (Figure S8). Thus, we describe these catalysts as Ni/La–Al–N and Co/La–Al–N in this paper. Notably, the La:N ratio approaches 3:3.2 for Ni/La–Al–N and 3:3.3 for Co/La–Al–N after annealing the used sample at 800 °C under Ar flow. These results suggest that a substantial quantity of nitrogen species are adsorbed on La–Al–N and especially the Co surface.

The amorphous-like XRD pattern and drastic increase of nitrogen content of used Ni- and Co-loaded La–Al–N suggest that the structure of La–Al–N is drastically modified from the original anti-perovskite structure. To discover the structure of La–Al–N, we first conducted STEM observations. As shown in the Figure S9, used Ni- and Co-loaded La–Al–N is severely distorted, and long-range orders of the crystal structure could not be confirmed. Moreover, the STEM-EDS observation showed that the Al is uniformly dispersed and clusters of LaN and Al could not be identified (Figure S1, Figure S10). Therefore, we subsequently annealed these samples at 800 °C under vacuum and studied the structure. Figure S11 shows the powder XRD patterns of annealed Ni/La–Al–N and Co/La–Al–N. In contrast to the used samples, the annealed sample shows broad peaks derived from rock-salt-type structure, in addition to Ni or Co, suggesting that La–Al–N possesses an almost identical structure compared to LaN. Meanwhile, peaks derived from Al species, such as Al and AlN, could not be identified even after heat treatment. The observed peaks of La–Al–N were much broader than *TM*/ReN reported previously, suggesting that Al species are doped into LaN. The XRD spectrum of annealed *TM*/La–Al–N remained largely unchanged after exposure to air for 1 hour. These data indicate that, while no peaks can be seen in the powder XRD, the local structure of La–Al–N is deduced to be similar to the rock-salt type LaN. Therefore, Ni- and Co-loaded La–Al–N show identical catalytic mechanism to *TM*/ReN for ammonia synthesis.

To further investigate the structure of La–Al–N, extended X-ray absorption fine structure (EXAFS) measurements at the La L$_3$-edge were conducted for used Ni/La–Al–N, used Co/La–Al–N, and the reference LaN. As shown in Figure 6, the EXAFS spectra of both Ni- and Co-loaded La–Al–N are well-explained by assuming that Al is doped into the La site of the rock-salt type structure, which are summarized in Table S1. The La–N radial distance was estimated to be 2.61 Å for pure LaN. Meanwhile, the La–N distances were reduced to 2.60 Å for Ni/La–Al–N and 2.57 Å for Co/La–Al–N. The reduced La–N bonding lengths are attributed to the smaller ionic radius

Angew. Chem. Int. Ed. **2022**, 61, e202211759 (5 of 7)

© 2022 Wiley-VCH GmbH
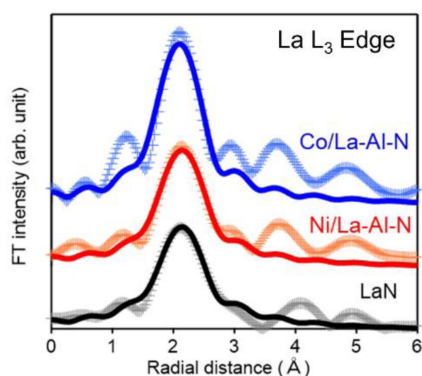
Figure 6. The EXAFS spectra of LaN, and used Ni- and Co-loaded La–Al–N. The cross points and solid lines represent experimental data points and theoretical fitting.

of Al compared to La, supporting our hypothesis that Al is doped into the La sites.

Next, we discuss how Al doping improves the moisture durability of the system. Density functional theory (DFT) calculations showed that the lattice parameter shrank when Al replaced partial La sites ($a = 5.144$ Å for $La_4Al_1N_4$; $a = 5.297$ Å for LaN), which is consistent with the EXAFS analysis. The nitrogen-vacancy formation energy (E_{NV}) is more enhanced in the 001 surface of $La_4Al_1N_4$ compared to that on pure LaN; i.e., the E_{NV}s were calculated as 1.92 eV for pure LaN and 3.15 eV for $La_4Al_1N_4$ (N bonded to Al). Accordingly, the energy modification of the hydrolysis reaction becomes smaller for $La_4Al_1N_4$ (Figure S12). Here, the energy changes of the hydrolysis reaction were defined as $E_{hydro} = E_{dis} - E_{La-Al-N/LaN} - E_{H2O}$, where E_{hydro} is the energy change of the hydrolysis reaction, E_{dis} is the free energy of the water-dissociated LaN (001) or La–Al–N (001) surface, $E_{La-Al-N/LaN}$ is the free energy of LaN (001) or La–Al–N (001) surface, and E_{H2O} is the free energy of a H_2O molecule. In the case of La–Al–N, two models were considered, in which dissociated H are located on N above La (denoted as La–Al–N_1) and Al (denoted as La–Al–N_2), respectively, as shown in Figure S12. The E_{hydro} value was estimated to be -1.73 eV (N above La) and -1.34 eV (N above Al) for La–Al–N, which are both higher than the value of pure LaN ($E_{hydro} = -1.84$ eV). These results show that H_2O-dissociated states become more unstable for La–Al–N and why Ni- and Co-loaded La–Al–N show higher chemical durability than pure LaN.

It should be noted that the local structure of NLa_6 coordination is unlikely affected after the La_3AlN transformation to La–Al–N. Despite the occurrence of significant lattice distortion caused by Al doping in the lattice, important catalytic properties, including reaction rates, activation energies, reaction orders, and isotope responses remain largely unchanged compared to ideal NRe_6 coordination of LaN and CeN supports, suggesting that ammonia synthesis over Ni/La–Al–N undergoes a similar reaction mechanism.

Finally, we compare the catalytic functionalities and mechanisms of the La–Al–N and other anti-perovskite-based materials. Notably, some of anti-perovskite nitrides have been investigated as nitrogen-storage materials, which

are highly efficient for ammonia synthesis by chemical looping. For example, Co_3ZnN, Ni_3ZnN, Co_3InN, and Ni_3InN were also reported as efficient nitrogen-storage materials.[44] Their lattice nitrogen efficiently reacts with feed H_2 and they transform to Co_3Zn, Ni_3Zn, Co_3In, and Ni_3In intermetallic phases after producing NH_3. Among them, Co_3ZnN and Ni_3ZnN exhibit high reaction rates and complete nitrogen release and ammonia production at 400–500°C. In comparison to the abovementioned systems, the original structure of La_3AlN transforms into Al-doped LaN upon loading of Ni and Co, and it serves as a thermal catalyst, which can continuously produce ammonia rather than the nitrogen carriers of looping. In either chemical looping or thermal catalytic processes, these findings show the usefulness of anti-perovskite nitrides and related compounds as platforms for ammonia synthesis.

Conclusion

In summary, we have presented a new Ni- and Co-loaded LaN-based catalyst with high chemical stability. While the catalytic mechanisms, such as activation energy and reaction orders, are similar to those of previously studied *TM/Re*N, the catalytic activity did not degrade even after exposure to moisture. During NH_3 synthesis, the La_3AlN anti-perovskite structure transformed to a La–Al–N distorted rock salt structure in which Al atoms are doped into the lattice of LaN. Even in this structure, the original functionalities of LaN were retained, while the La–Al bonding protected the catalyst from oxidation. DFT calculations revealed that absorption and O–H dissociation of H_2O molecule were hindered after Al doping, realizing a more chemically durable surface. The remarkable stability and catalytic activity, alongside the use of precious-metal-free elements, such as Ni and Co, distinguishes *TM*/La–Al–N among the various heterogeneous catalysts for ammonia synthesis. These results highlight the importance of metal–metal bonding during the material design and thus provide additional degrees of freedom for the design of heterogeneous catalysts for ammonia synthesis.

Conflict of Interest

The authors declare no conflict of interest.

Data Availability Statement

The data that support the findings of this study are available from the corresponding author upon reasonable request.

[1] T. Kandemir, M. E. Schuster, A. Senyshyn, M. Behrens, R. Schlögl, *Angew. Chem. Int. Ed.* **2013**, *52*, 12723–12726; *Angew. Chem.* **2013**, *125*, 12955–12959.

[2] S. Gambarotta, J. Scott, *Angew. Chem. Int. Ed.* **2004**, *43*, 5298–5308; *Angew. Chem.* **2004**, *116*, 5412–5422.

[3] G. Ertl, *Angew. Chem. Int. Ed. Engl.* **1990**, *29*, 1219–1227; *Angew. Chem.* **1990**, *102*, 1258–1266.

[4] M. Kitano, Y. Inoue, Y. Yamazaki, F. Hayashi, S. Kanbara, S. Matsuishi, T. Yokoyama, S. W. Kim, M. Hara, H. Hosono, *Nat. Chem.* **2012**, *4*, 934–940.

[5] H. Hosono, M. Kitano, *Chem. Rev.* **2021**, *121*, 3121–3185.

[6] M. Hara, M. Kitano, H. Hosono, *ACS Catal.* **2017**, *7*, 2313–2324.

[7] J. Kammert, J. Moon, Y. Cheng, L. Daemen, S. Irle, V. Fung, J. Liu, K. Page, X. Ma, V. Phaneuf, J. Tong, A. J. Ramirez-Cuesta, Z. Wu, *J. Am. Chem. Soc.* **2020**, *142*, 7655–7667.

[8] Y. Toda, H. Yanagi, E. Ikenaga, J. J. Kim, M. Kobata, S. Ueda, T. Kamiya, M. Hirano, K. Kobayashi, H. Hosono, *Adv. Mater.* **2007**, *19*, 3564–3569.

[9] S. Kanbara, M. Kitano, Y. Inoue, T. Yokoyama, M. Hara, H. Hosono, *J. Am. Chem. Soc.* **2015**, *137*, 14517–14524.

[10] M. Kitano, S. Kanbara, Y. Inoue, N. Kuganathan, P. V. Sushko, T. Yokoyama, M. Hara, H. Hosono, *Nat. Commun.* **2015**, *6*, 6731.

[11] Y. Lu, J. Li, T. Tada, Y. Toda, S. Ueda, T. Yokoyama, M. Kitano, H. Hosono, *J. Am. Chem. Soc.* **2016**, *138*, 3970–3973.

[12] J. Wu, Y. Gong, T. Inoshita, D. C. Fredrickson, J. Wang, Y. Lu, M. Kitano, H. Hosono, *Adv. Mater.* **2017**, *29*, 1700924.

[13] M. Kitano, Y. Inoue, H. Ishikawa, K. Yamagata, T. Nakao, T. Tada, S. Matsuishi, T. Yokoyama, M. Hara, H. Hosono, *Chem. Sci.* **2016**, *7*, 4036–4043.

[14] K. Aika, K. Shimazaki, Y. Hattori, A. Ohya, S. Ohshima, K. Shirota, A. Ozaki, *J. Catal.* **1985**, *92*, 296–304.

[15] A. Ozaki, K. Aika, H. Hori, *Bull. Chem. Soc. Jpn.* **1971**, *44*, 3216–3216.

[16] M. Nishi, S. Chen, H. Takagi, *Catalysts* **2019**, *9*, 480.

[17] M. Muhler, F. Rosowski, O. Hinrichsen, A. Hornung, G. Ertl, *Stud. Surf. Sci. Catal.* **1996**, *101A*, 317–326.

[18] C. J. H. Jacobsen, S. Dahl, B. G. S. Clausen, S. Bahn, A. Logadottir, J. K. Nørskov, *J. Am. Chem. Soc.* **2001**, *123*, 8404–8405.

[19] J. Nørskov, J. Chen, R. Miranda, T. Fitzsimmons, R. Stack, *Sustainable Ammonia Synthesis—Exploring the Scientific Challenges Associated with Discovering Alternative, Sustainable Processes for Ammonia Production* **2016**, https://doi.org/10.2172/1283146.

[20] A. Vojvodic, J. K. Nørskov, *Natl. Sci. Rev.* **2015**, *2*, 140–143.

[21] A. J. Medford, A. Vojvodic, J. S. Hummelshøj, J. Voss, F. Abild-Pedersen, F. Studt, T. Bligaard, A. Nilsson, J. K. Nørskov, *J. Catal.* **2015**, *328*, 36–42.

[22] P. Wang, H. Xie, J. Guo, Z. Zhao, X. Kong, W. Gao, F. Chang, T. He, G. Wu, M. Chen, L. Jiang, P. Chen, *Angew. Chem. Int. Ed.* **2017**, *56*, 8716–8720; *Angew. Chem.* **2017**, *129*, 8842–8846.

[23] P. Wang, F. Chang, W. Gao, J. Guo, G. Wu, T. He, P. Chen, *Nat. Chem.* **2017**, *9*, 64–70.

[24] X. Wang, X. Peng, W. Chen, G. Liu, A. Zheng, L. Zheng, J. Ni, C. T. Au, L. Jiang, *Nat. Commun.* **2020**, *11*, 653.

[25] Y. Zhou, C. Q. Xu, Z. Tan, H. Cai, X. Wang, J. Li, L. Zheng, C. T. Au, J. Li, L. Jiang, *ACS Catal.* **2022**, *12*, 2651–2660.

[26] L. Li, T. Zhang, J. Cai, H. Cai, J. Ni, B. Lin, J. Lin, X. Wang, L. Zheng, C. T. Au, L. Jiang, *J. Catal.* **2020**, *389*, 218–228.

[27] C. D. Zeinalipour-Yazdi, J. S. J. Hargreaves, C. R. A. Catlow, *J. Phys. Chem. C* **2018**, *122*, 6078–6082.

[28] N. Bion, F. Can, J. Cook, J. S. J. Hargreaves, A. L. Hector, W. Levason, A. R. McFarlane, M. Richard, K. Sardar, *Appl. Catal. A* **2015**, *504*, 44–50.

[29] N. J. Lawrence, J. R. Brewer, L. Wang, T. S. Wu, J. Wells-Kingsbury, M. M. Ihrig, G. Wang, Y. L. Soo, W. N. Mei, C. L. Cheung, *Nano Lett.* **2011**, *11*, 2666–2671.

[30] F. Esch, S. Fabris, L. Zhou, T. Montini, C. Africh, P. Fornasiero, G. Comelli, R. Rosei, *Science* **2005**, *309*, 752–755.

[31] C. T. Campbell, C. H. F. Peden, *Science* **2005**, *309*, 713–714.

[32] T. N. Ye, S. W. Park, Y. Lu, J. Li, M. Sasase, M. Kitano, T. Tada, H. Hosono, *Nature* **2020**, *583*, 391–395.

[33] T. N. Ye, S. W. Park, Y. Lu, J. Li, M. Sasase, M. Kitano, H. Hosono, *J. Am. Chem. Soc.* **2020**, *142*, 14374–14383.

[34] F. Stegemann, O. Janka, *Dalton Trans.* **2016**, *45*, 13863–13871.

[35] J. Wu, J. Li, Y. Gong, M. Kitano, T. Inoshita, H. Hosono, *Angew. Chem. Int. Ed.* **2019**, *58*, 825–829; *Angew. Chem.* **2019**, *131*, 835–839.

[36] J. Li, J. Wu, H. Wang, Y. Lu, T. Ye, M. Sasase, X. Wu, M. Kitano, T. Inoshita, H. Hosono, *Chem. Sci.* **2019**, *10*, 5712–5718.

[37] T. Nakano, S. Onuki, N. Takeda, *Phys. C* **2013**, *493*, 109–111.

[38] M. Kirchner, F. Gäbler, W. Schnelle, F. R. Wagner, R. Niewa, *Z. Kristallogr. - Cryst. Mater.* **2006**, *221*, 543–553.

[39] G. Cacciamani, R. Ferro, *CALPHAD Comput. Coupling Phase Diagrams Thermochem* **2001**, *25*, 583–597.

[40] L. Jin, Y. B. Kang, P. Chartrand, C. D. Fuerst, *CALPHAD Comput. Coupling Phase Diagrams Thermochem* **2011**, *35*, 30–41.

[41] T. N. Ye, S. W. Park, Y. Lu, J. Li, J. Wu, M. Sasase, M. Kitano, H. Hosono, *J. Am. Chem. Soc.* **2021**, *143*, 12857–12866.

[42] M. Kitano, J. Kujirai, K. Ogasawara, S. Matsuishi, T. Tada, H. Abe, Y. Niwa, H. Hosono, *J. Am. Chem. Soc.* **2019**, *141*, 20344–20353.

[43] Q. Wang, J. Pan, J. Guo, H. A. Hansen, H. Xie, L. Jiang, L. Hua, H. Li, Y. Guan, P. Wang, W. Gao, L. Liu, H. Cao, Z. Xiong, T. Vegge, P. Chen, *Nat. Catal.* **2021**, *4*, 959–967.

[44] Y. Goto, A. Daisley, J. S. J. Hargreaves, *Catal. Today* **2021**, *364*, 196–201.